Nuclear Engineering and Technology 53 (2021) 3784–3789

Contents lists available at ScienceDirect

Nuclear Engineering and Technology

journal homepage: www.elsevier.com/locate/net

Original Article

Neutron spectroscopy using pure $LaCl_3$ crystal and the dependence of pulse shape discrimination on Ce-doped concentrations

Phan Quoc Vuong [a], Hongjoo Kim [a, *], Nguyen Thanh Luan [a], Sunghwan Kim [b]

[a] Department of Physics, Kyungpook National University, 41566, Daegu, South Korea
[b] Department of Radiological Science, Cheongju University, 28503, Cheongju, South Korea

ARTICLE INFO

Article history:
Received 7 October 2020
Received in revised form
14 May 2021
Accepted 17 May 2021
Available online 21 May 2021

Keywords:
Neutron spectroscopy
Pure $LaCl_3$ crystal
Pulse shape discrimination
Dual gamma/Neutron detection

ABSTRACT

We report a simple technique for direct neutron spectroscopy using pure $LaCl_3$ crystals. Pure $LaCl_3$ crystals exhibit considerably better pulse shape discrimination (PSD) capabilities with relatively good energy resolution as compared with Ce-doped $LaCl_3$ crystals. Single crystals of pure and Ce-doped $LaCl_3$ were grown using an inhouse-developed Bridgman furnace. PSD capabilities of these crystals were investigated using ^{241}Am and ^{137}Cs sources. Fast neutron detection was tested using a ^{252}Cf source and three separate bands corresponding to electron, proton, and alpha were observed. The proton band induced by the $^{35}Cl(n,p)^{35}S$ reaction can be used for direct neutron spectroscopy because proton energy is proportional to incident neutron energy. Owing to good scintillation performance and excellent PSD capabilities, pure $LaCl_3$ is a promising candidate for space detectors and other applications that necessitate gamma/fast neutron discrimination capability.

1. Introduction

Recently, the development of fast neutron detection using Cs_2LiYCl_6:Ce (CLYC) crystals has revealed a new method of using Cl containing crystals with excellent pulse shape discrimination (PSD) capability for neutron spectroscopy [1,2]. CLYC crystals have been examined for many applications requiring dual mode gamma/neutron capability with better energy resolution than the conventional NaI:Tl detectors. Fast neutron detection using CLYC crystals is possible because of $^{35}Cl(n,p)^{35}S$ and $^{35}Cl(n,\alpha)^{32}P$ reactions with significant cross sections. Incident neutron energies below 4 MeV can be directly measured because they are proportional to the energy of charged-particle products [3]. This new method is simpler than traditional time-of-flight and unfolding techniques using Boner sphere spectrometer or liquid scintillators. In addition, the detector is more compact than that used in other techniques. Therefore, CLYC has been considered for many applications such as neutron scattering in nuclear physics experiments [4], near-space neutron detection [5], homeland security [6], deuterium plasma diagnostics [7], and well-logging [8].

In spite of these many advantages, CLYC cannot separate alpha and proton particles using the PSD methods [9]. Therefore, extrapolating the neutron energy information from the overlapped spectra is challenging. The degradation of scintillation performance due to radiation damage is another disadvantage of CLYC [10] in applications such as space-based detectors. Hence, suitable alternatives have been pursued by scanning many Cl containing scintillators grown by our group, such as $SrCl_2$ [11], $Ba_xSr_{(1-x)}Cl_2$ [12], Tl_2ZrCl_6 [13,14], $LaCl_3$, $TlLa_2Cl_5$ [15], and $Cs_2LiCeCl_6$ [16]. Among them, pure $LaCl_3$ exhibited excellent PSD capability with good radiation hardness, which has already been reported elsewhere [17]. Moreover, $LaCl_3$ crystal (3.84 g/cm^3) has higher density than CLYC crystal (3.31 g/cm^3) so that its chloride density is 1.36 times higher than that of CLYC crystal.

The state-of-the-art lanthanide-doped scintillators were intensively explored in the early twenty-first century [18]. Ce-doped $LaCl_3$ crystals exhibit excellent scintillation performance with an energy resolution of 3.3% FWHM at 662 keV. Pure $LaCl_3$ crystals also show good light yield of 34,000 photons/MeV and energy resolution of 4.7% [19]. However, $LaCl_3$ crystals gain less practical attention owing to their slower decay than Ce-doped crystals. The self-trapped exciton (STE) is the scintillation origin of pure $LaCl_3$ as it is for many other halide crystals [20]. The contribution of STE to total light yield of $LaCl_3$:Ce is reduced with an increase in the Ce dopant concentration owing to energy transfer from STE to the Ce^{3+} center [21]. $LaCl_3$:Ce shows modest PSD capability with a

* Corresponding author.
E-mail address: hongjoo@knu.ac.kr (H. Kim).

https://doi.org/10.1016/j.net.2021.05.020

discrepancy in the literature because of the dependence of the discrimination power on the Ce^{3+} concentration [22–24].

In this study, PSD capability of pure $LaCl_3$ crystals was investigated. To understand the role of Ce dopant concentration in PSD, several $LaCl_3$ crystals doped with small amounts of Ce were prepared. Moreover, fast neutron detection capability of the pure $LaCl_3$ crystal was demonstrated using a weak ^{252}Cf source.

2. Experimental

For sample preparation, ultradry 4 N purity $LaCl_3$ beads and 4 N purity $CeCl_3$ powder (APL Engineered Materials, Inc., USA) were used. Ce-doped and pure LaCl3 were weighted and loaded into precleaned and backed quartz ampoules with inner diameter of 8 mm and 15 mm, respectively. This process was done inside a dry glove box filled with argon to avoid degradation of the starting materials. The materials were further dried to remove any residual moisture at 230 °C under dynamic evacuation for 24 h. The ampoules were sealed using oxygen propane torch. The single crystals of pure and 0.01, 0.05, and 0.1 at. % Ce-doped $LaCl_3$ were grown at a pulling rate of 0.5 mm/h and thermal gradient of approximately 20 °C/cm using an inhouse developed Bridgman furnace. The inset of Fig. 1 shows the crack-free Ø15-mm pure $LaCl_3$ crystal. Four samples of pure and Ce-doped $LaCl_3$ were cut and polished for characterization inside a glove box to avoid degradation during measurements. The samples were wrapped with several layer of 0.2 mm Teflon sheet, except one facet for coupling with a R6233-100 photomultiplier tube (PMT), (Hamamatsu, Japan) using optical grease.

The PSD capabilities of pure and Ce-doped LaCl crystals for alpha and gamma signals were studied using ^{137}Cs and ^{241}Am sources. The analog output signals from the PMT were digitized using an FADC400 (Notice Company, Korea) with a resolution of 10 bits and maximum sampling rate of 400 MS/s. The recorded pulses were analyzed for scintillation decay time and PSD using a customized C++ code [25] compiled and run in a ROOT package. The pulse height spectrum of the pure $LaCl_3$ crystal acquired using the ^{137}Cs source is presented in Fig. 1. In this study, an integration time of 10 μs was selected for the rest of the pulse height calculation. A good energy resolution of 4.0% at 662 keV was obtained for the Ø15 × 15 mm^3 pure $LaCl_3$ crystal.

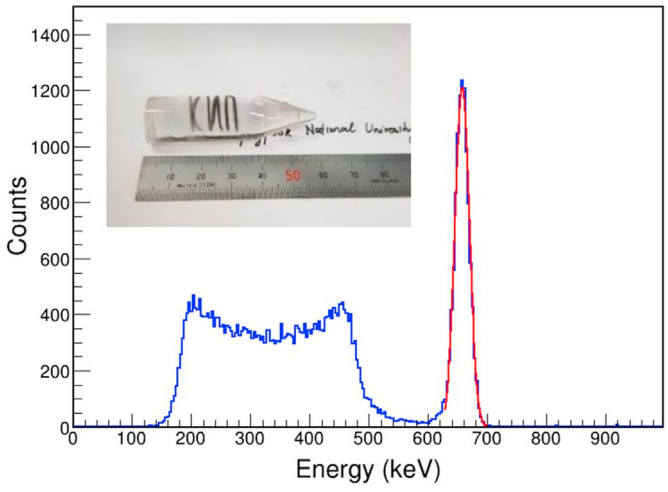

Fig. 1. Pulse height spectrum measured using a ^{137}Cs source of a pure $LaCl_3$ crystal. The energy resolution was estimated to be 4.0% at 662 keV. The inset shows the Ø15-mm pure $LaCl_3$ crystal grown using Bridgman furnace.

3. Decay time and pulse shape discrimination

In the case of pure $LaCl_3$ crystal, the scintillation decay times under alpha excitation were significantly faster than those under gamma excitation, as shown in Fig. 2a. We attempted to shorten the decay time to maintain good alpha/gamma separation by doping $LaCl_3$ with small amounts of Ce. However, the differences between alpha and gamma decay signals was dramatically less even using a very small Ce dopant concentration of 0.01 at. %, as shown in Fig. 2b. These values further reduced at 0.05% and 0.1% Ce dopant concentration such that they were nearly indistinguishable, as shown in Fig. 2c and d, respectively.

The charge comparison method was used for the PSD study of the pure and Ce-doped $LaCl_3$ crystals. In this method, two time gates corresponding to fast and slow scintillation decays were selected. The PSD ratios, i.e., the ratios of the collected charge within the prompt (C_p) and delay gates (C_d), were calculated for comparison.

$$\text{PSD ratio} = \frac{C_p}{C_p + C_d}. \quad (1)$$

The PSD ratio distribution for alpha and gamma signals from the ^{137}Cs and ^{241}Am sources is presented in Fig. 3. The peaks were fitted with Gaussian function to estimate the figure-of-merit (FOM), a parameter shows the separation power between alpha and gamma signals. The FOM is a function of the peak position and FWHM with the form:

$$\text{FOM} = \frac{|P_\alpha - P_\gamma|}{FWHM_\alpha + FWHM_\gamma}. \quad (2)$$

The prompt and delay gate were optimized to obtain the best FOM values for both pure and Ce-doped $LaCl_3$ crystals. The FOM values were calculated using a customized C++ program for each pair prompt and delay gates in a matrix with the interval of 20 ns and 100 ns, respectively, as shown in Fig. 4. The best FOM values were estimated to be 2.5, 1.8, 0.9, and 0.8 for pure, 0.01%, 0.05%, and 0.1% Ce-doped LaCl3 crystals, respectively. Only one maximum FOM peak ascribed to STE was observed for the pure and 0.01% Ce-doped $LaCl_3$ crystals, as shown in Fig. 4a and b, while a second peak appeared at the bottom-left corner for the 0.05% Ce-doped $LaCl_3$ crystal and became dominant for 0.1% Ce-doped $LaCl_3$ crystal, as shown in Fig. 4c and d. The second peak corresponds to the fast decay of the Ce^{3+} luminescence center. The STE-related peak faded and shifted from the bottom-right corner to the upper left with increasing Ce concentrations. The observed phenomena were attributed to the energy transfer from STE to Ce^{3+}, which shortened the decay time of the STE component and reduced its contribution to the total light yield [21].

The PSD matrices were reconstructed for gamma and alpha events obtained from the ^{137}Cs and ^{241}Am sources using the optimized time gates, as shown in Fig. 5. The alpha peaks were broad because of a degraded layer on the crystal surface. The α/β ratios were roughly estimated to be 0.2, 0.24, 0.25 and 0.28 for pure, 0.01%, 0.05%, and 0.1% Ce-doped LaCl3 crystals, respectively. The increasing trend of the α/β ratio was attributed to the increase in Ce^{3+}, which can provide slightly more efficient luminescence decay paths for the very high excitation density of the alpha particles. The alpha/gamma separation of the Ce-doped $LaCl_3$ crystals was modest, which is insufficient for fast neutron detection [24]. Therefore, only pure $LaCl_3$ was selected for fast neutron measurements.

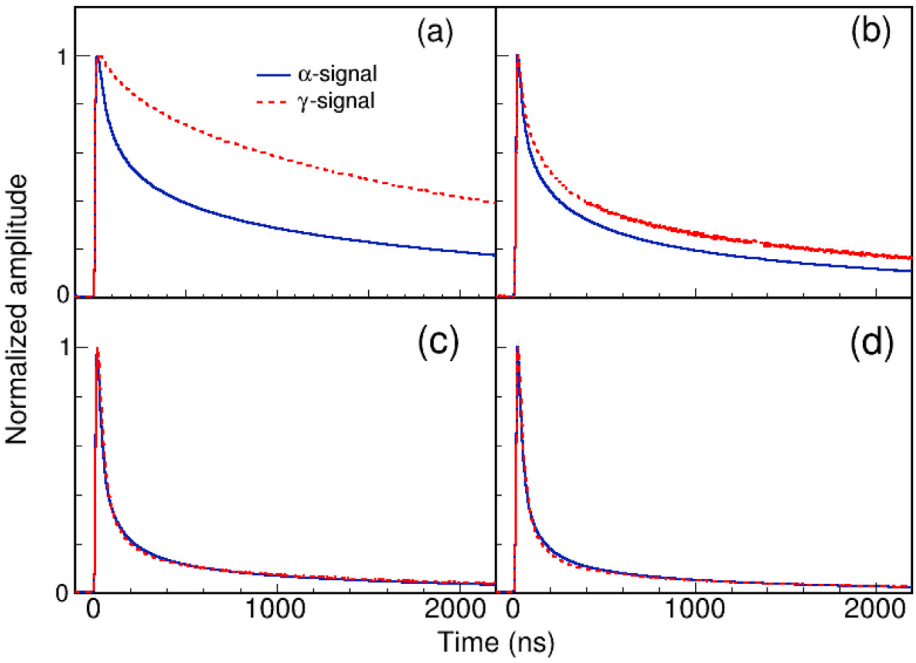

Fig. 2. Normalized scintillation decay under gamma (blue line) and alpha (red dash) excitation. The biggest gamma/alpha separation was observed for the pure $LaCl_3$ crystal (a) and reduced with Ce concentrations of 0.01% (b), 0.05% (c), and 0.1% (d). (For interpretation of the references to colour in this figure legend, the reader is referred to the Web version of this article.)

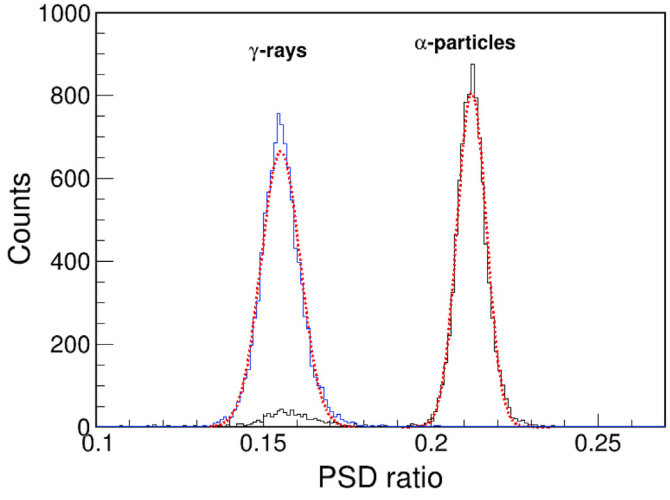

Fig. 3. The PSD ratio distribution of gamma and alpha events from ^{137}Cs and ^{241}Am sources, respectively. The peaks were fitted with Gausian function for computing the FOM.

4. Fast neutron measurement

For fast neutron measurements, the pure $LaCl_3$ sample was encapsulated to measure a weak ^{252}Cf source. The measurement was performed for two days to achieve a reasonable statistic owing to the low neutron activity of the source. The pulse height spectrum was obtained as shown in Fig. 6a. Several dominant gamma peaks were observed, including peaks at 388, 662, and 1436 keV from ^{249}Cf, ^{137}Cs (fission products), and ^{138}La (internal background) isotopes [26], respectively. This finding agrees well with the characteristics of an aged ^{252}Cf source [27].

The scatter plot of the events obtained from the ^{252}Cf source is shown in Fig. 6b. Two clear separate bands appearing above the gamma band were observed. The band with the highest PSD ratio was corresponded to the alpha events generated because of the $^{35}Cl(n,\alpha)^{32}P$ reaction and internal alpha background from the ^{227}Ac decay chain [26]. To confirm that the background measurement was performed, an isolated alpha band was observed, as shown in Fig. 6c. The band located between the gamma and alpha bands presented proton events generated because of the $^{35}Cl(n,p)^{35}S$ reactions.

There is a dependence of the PSD ratio on the alpha and proton energies, while it was considerably stable for the gamma rays. The PSD ratios of both alpha and proton bands decreased when their energy levels increased. It is caused by the luminescence quenching which influences the charged particle separation capability of the pure $LaCl_3$ crystal. The luminescence quenching can be quantitatively estimated by quenching factor that equal to the electron equivalent energy per the actual energy of charge particles [28]. For example, the quenching factor significantly increased from 0.2 at 5.4 MeV (^{241}Am) to 0.29 at 7.4 MeV (alpha events from the pure alpha decay of ^{215}Po isotope [23]). Thus, when the ionization density increased, more nonradiative recombination occurred, reducing the contribution of the long decay component to the total light yield. Because the ionization density of the charged particles increases when energies decreases, the PSD ratio was higher in the lower energy region.

The electron equivalent energy spectrum of the proton events is shown in Fig. 5d; this spectrum has a shape similar to that of the spontaneous fission neutron spectrum obtained from the ^{252}Cf source. The neutron energy information can be extrapolated if the quenching factor of proton signals is known, which can be measured using monoenergetic neutron beams. This indicates that neutron spectroscopy can be realized using pure $LaCl_3$ crystals. The inset of Fig. 6d presents the projection on the y axis of the selected events in the red box shown in Fig. 6b. For the separation of alpha with the other particles, the energy range of 1920 keVee to 2230 keVee was selected because it cover the pure alpha peak from ^{215}Po isotope. The PSD ratio distribution of electron, proton and alpha

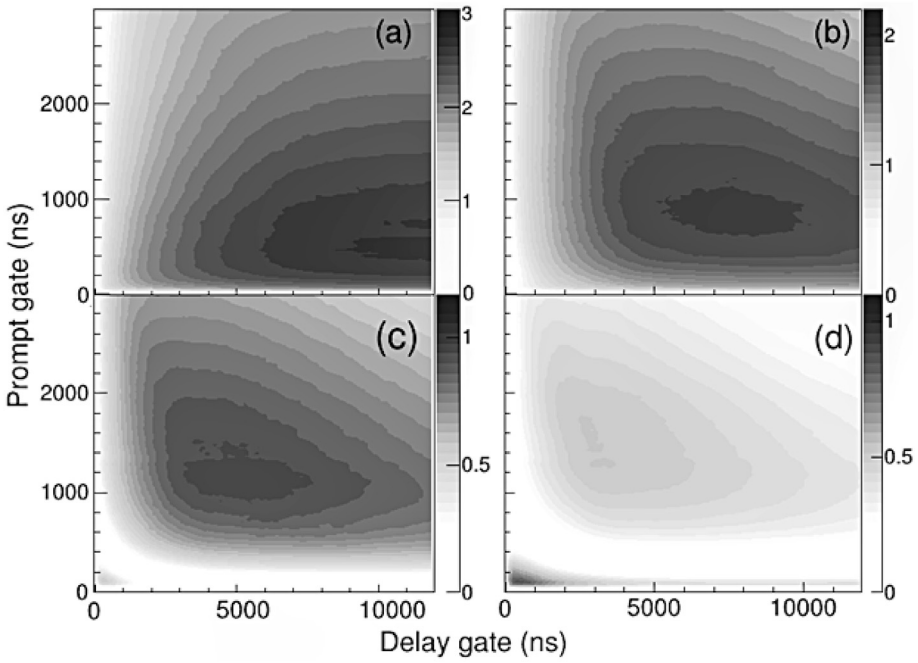

Fig. 4. Contour plots of the FOM as a function of prompt and delay gates for pure (a), 0.01% (b), 0.05% (c), and 0.1% (d) Ce-doped $LaCl_3$ crystals.

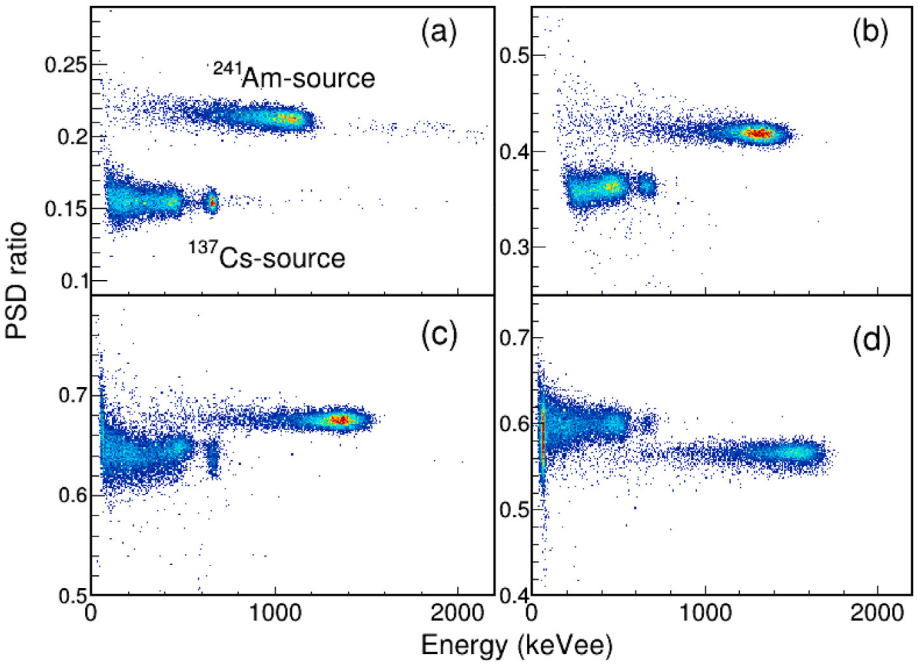

Fig. 5. The scatter plot of the PSD ratio versus gamma equivalent energy under optimized conditions for pure (a), 0.01% (b), 0.05% (c), and 0.1% (d) Ce-doped $LaCl_3$ crystals.

events was fitted with Gaussian functions. The fitted parameters were used to estimate the FOM values, which were found to be 2.02, 1.95 and 3.95 for alpha/proton, proton/electron, and alpha/electron separation, respectively. These values are considerably higher than the minimum required FOM value (1.5) for practical applications [29].

5. Conclusion

The $LaCl_3$ crystals were easy to grow using the Bridgman technique which is favorable for mass production. An energy resolution of 4.0% was obtained at 662 keV for the Ø15 × 15 mm pure $LaCl_3$ crystal. It showed excellent PSD capability for the practical use of fast neutron spectroscopy compared with the Ce-doped $LaCl_3$ crystals. The obtained FOM values were found to be 2.02, 1.95 and 3.95 for alpha/proton, proton/electron, and alpha/electron separation, respectively. Fast neutron measurements using an aged ^{252}Cf source were also performed. The proton band attributed to the $^{35}Cl(n,\alpha)^{32}P$ reaction is a promising candidate for direct spectroscopy of low energy neutrons. Moreover, fast neutron detection

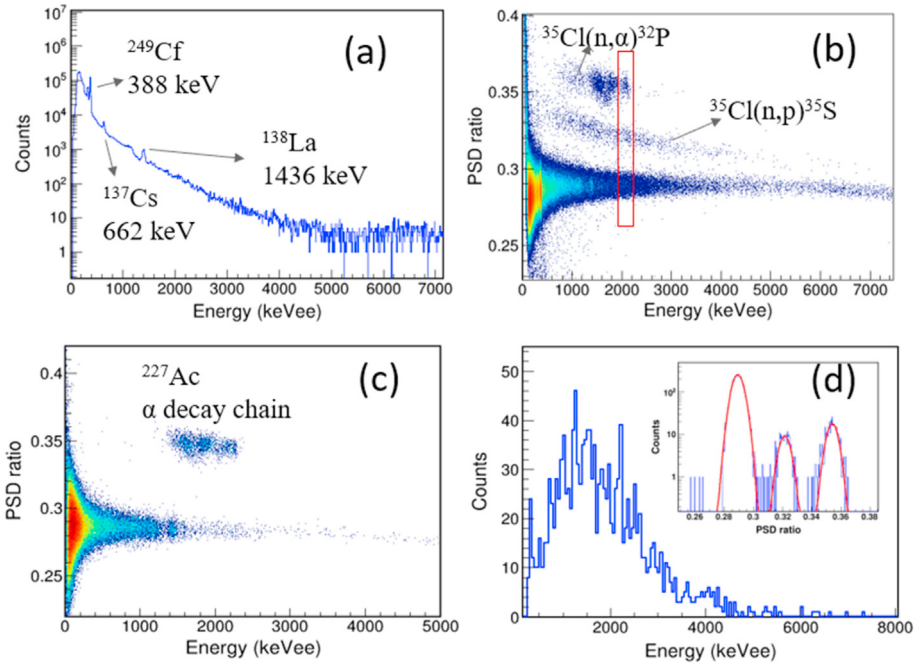

Fig. 6. (a) Pulse height spectra acquired using an aged ^{252}Cf source showing several intense gamma peaks from its fission products. The scatter plot of the PSD ratio versus gamma equivalent energy of incident particles for the (b) ^{252}Cf source and (c) background measurement. (d) The projection of proton events on x-axis and the inset shows the projection of selected events in the red box of the plot (c) on the y axis. The alpha, proton, and gamma peaks were fitted with Gaussian functions for estimating FOM. (For interpretation of the references to colour in this figure legend, the reader is referred to the Web version of this article.)

efficiency of the $LaCl_3$ was significantly higher than that of the CLYC crystal because its chloride density is 1.36 times higher than that of the CLYC crystal. Owing to its excellent scintillation performance, the pure $LaCl_3$ crystal can be considered as a replacement for the ^{7}Li-enriched CLYC crystal in many applications such as neutron monitoring and water exploration in space, nuclear physics experiments, well-logging, homeland security.

Declaration of competing interest

The authors declare that they have no known competing financial interests or personal relationships that could have appeared to influence the work reported in this paper.

Acknowledgments

The study was supported by the National Research Foundation of Korea (NRF), funded by the Ministry of Science and Technology, Korea (MEST), (No.2018R1A2A1A05022079 and No. 2020R1I1A1A01068102).

References

[1] M.B. Smith, T. Achtzehn, H.R. Andrews, E.T.H. Clifford, H. Ing, V.D. Kovaltchouk, Fast neutron spectroscopy using Cs_2LiYCl_6:Ce (CLYC) scintillator, IEEE Trans. Nucl. Sci. 60 (2013) 855–859.
[2] N. D'Olympia, P. Chowdhury, C.J. Guess, T. Harrington, E.G. Jackson, S. Lakshmi, C.J. Lister, J. Glodo, R. Hawrami, K. Shah, U. Shirwadkar, Optimizing Cs_2LiYCl_6 for fast neutron spectroscopy, Nucl. Instrum. Methods Phys. Res. A. 694 (2012) 140–146.
[3] N. Dolympia, P. Chowdhury, E.G. Jackson, C.J. Lister, Fast neutron response of ^{6}Li-depleted CLYC detectors up to 20 MeV, Nucl. Instrum. Methods Phys. Res. A. 763 (2014) 433–441.
[4] T. Brown, P. Chowdhury, E. Doucet, E.G. Jackson, C.J. Lister, A.J. Mitchell, C. Morse, A.M. Rogers, G.L. Wilson, N. D'Olympia, M. Devlin, N. Fotiades, J.A. Gomez, S.M. Mosby, R.O. Nelson, Applications of C^7LYC scintillators in fast neutron spectroscopy, Nucl. Instrum. Methods Phys. Res. A. 954 (2020) 161123.
[5] D.J. Lawrence, S. Fix, J.O. Goldsten, S.V. Heuer, R.S. Hourani, S. Kerem, P.N. Peplowski, Near-space operation of compact CsI, CLYC, and $CeBr_3$ sensors: results from two high-altitude balloon flights, Nucl. Instrum. Methods Phys. Res. A 905 (2018) 33–46.
[6] L. Soundara-Pandian, J. Tower, C. Hines, P. O'Dougherty, J. Glodo, K. Shah, Characterization of large volume CLYC scintillators for nuclear security applications, IEEE Trans. Nucl. Sci. 64 (2017) 1744–1748.
[7] G. Ericsson, Advanced neutron spectroscopy in fusion Research, J. Fusion Energy 38 (2019) 330–355.
[8] Q. Zhang, F. Zhang, R.P. Gardner, H. Yan, G. Wu, L. Tian, Q. Chen, Y. Ti, A method for determining density based on gamma ray and fast neutron detection using a Cs_2LiYCl_6 detector in neutron-gamma density logging, Appl. Radiat. Isot. 142 (2018) 77–84.
[9] N. Blasi, S. Brambilla, F. Camera, S. Ceruti, A. Giaz, L. Gini, F. Groppi, S. Manenti, A. Mentana, B. Million, S. Riboldi, Fast neutron detection efficiency of ^{6}Li and ^{7}Li enriched CLYC scintillators using an Am-Be source, J. Instrum. 13 (2018) 11010.
[10] K.E. Mesick, K.D. Bartlett, D.D.S. Coupland, L.C. Stonehill, Effects of proton-induced radiation damage on CLYC and CLLBC performance, Nucl. Instrum. Methods Phys. Res. A. 948 (2019) 1–22.
[11] G. Rooh, H. Kang, H.J. Kim, H. Park, S.H. Doh, Scintillation characteristics of the $SrCl_2$ single crystal for the neutrinoless β^+/EC decay search, IEEE Trans. Nucl. Sci. 55 (2008) 1445–1448.
[12] J. Kim, H. Kang, H.J. Kim, H. Park, S. Kim, S. Doh, Scintillation properties of $Ba_xSr_{1-x}Cl_2$ single crystals, IEEE Trans. Nucl. Sci. 55 (2008) 1464–1468.
[13] Q.V. Phan, H.J. Kim, G. Rooh, S.H. Kim, Tl_2ZrCl_6 crystal: efficient scintillator for X- and γ-ray spectroscopies, J. Alloys Compd. 766 (2018) 326–330.
[14] P. Bhattacharya, C. Brown, C. Sosa, M. Wart, S. Miller, C. Brecher, V.V. Nagarkar, Tl_2ZrCl_6 and Tl_2HfCl_6 intrinsic scintillators for gamma rays and fast neutron detection, IEEE Trans. Nucl. Sci. 67 (2020) 1032–1034.
[15] A. Khan, P.Q. Vuong, G. Rooh, H.J. Kim, S. Kim, Crystal growth and Ce^{3+} concentration optimization in Tl_2LaCl_5: an excellent scintillator for the radiation detection, J. Alloys Compd. 827 (2020) 154366.
[16] G. Rooh, H.J. Kim, S. Kim, Study on crystal growth and scintillation characteristics of $Cs_2LiCeCl_6$, IEEE Trans. Nucl. Sci. 57 (2010) 1255–1259.
[17] P.F. Bloser, M.L. McConnell, J.R. Macri, P.J. Bruillard, J.M. Ryan, W. Hajdas, Radiation damage and activation from proton irradiation of advanced scintillators, IEEE Nucl. Sci. Symp. Conf. Rec. 3 (2006) 1500–1505.
[18] E.V.D. Van Loef, P. Dorenbos, C.W.E. Van Eijk, K. Krämer, H.U. Güdel, High-energy-resolution scintillator: Ce^{3+} activated $LaBr_3$, Appl. Phys. Lett. 79 (2001) 1573–1575.
[19] E.V.D. Van Loef, P. Dorenbos, C.W.E. Van Eijk, K. Krämer, H.U. Güdel, Scintillation properties of $LaCl_3$:Ce^{3+} crystals: fast, efficient, and high-energy resolution scintillators, in: IEEE Trans. Nucl. Sci., 2001, pp. 341–345.
[20] G. Bizarri, P. Dorenbos, Temperature dependent scintillation properties of pure $LaCl_3$, J. Phys. Condens. Matter 21 (2009).
[21] E.V.D. Van Loef, P. Dorenbos, C.W.E. Van Eijk, The scintillation mechanism in

$LaCl_3:Ce^{3+}$, J. Phys. Condens. Matter 15 (2003) 1367–1375.
[22] F.C.L. Crespi, F. Camera, N. Blasi, A. Bracco, S. Brambilla, B. Million, R. Nicolini, L. Pellegri, S. Riboldi, M. Sassi, O. Wieland, F. Quarati, A. Owens, Alpha-gamma discrimination by pulse shape in $LaBr_3$:Ce and $LaCl_3$:Ce, Nucl. Instrum. Methods Phys. Res. A. 602 (2009) 520–524.
[23] W. Wolszczak, P. Dorenbos, Shape of intrinsic alpha pulse height spectra in lanthanide halide scintillators, Nucl. Instrum. Methods Phys. Res. A. 857 (2017) 66–74.
[24] M.P. Taggart, J. Henderson, Fast-neutron response of $LaBr_3$(Ce) and $LaCl_3$(Ce) scintillators, Nucl. Instrum. Methods Phys. Res. A. 975 (2020) 1–5.
[25] P.Q. Vuong, H.J. Kim, H. Park, G. Rooh, S.H. Kim, Pulse shape discrimination study with Tl_2ZrCl_6 crystal scintillator, Radiat. Meas. 123 (2019) 83–87.
[26] B.D. Milbrath, R.C. Runkle, T.W. Hossbach, W.R. Kaye, E.A. Lepel, B.S. McDonald, L.E. Smith, Characterization of alpha contamination in lanthanum trichloride scintillators using coincidence measurements, Nucl. Instrum. Methods Phys. Res. A. 547 (2005) 504–510.
[27] R.J. Gehrke, R. Aryaeinejad, J.K. Hartwell, W.Y. Yoon, E. Reber, J.R. Davidson, The γ-ray spectrum of ^{252}Cf and the information contained within it, Nucl. Instrum. Methods Phys. Res. Sect. B Beam Interact. Mater. Atoms 213 (2004) 10–21.
[28] H.W. Joo, H.S. Park, J.H. Kim, J.Y. Lee, S.K. Kim, Y.D. Kim, H.S. Lee, S.H. Kim, Quenching factor measurement for NaI(Tl) scintillation crystal, Astropart. Phys. 108 (2019) 50–56.
[29] R.A. Winyard, J.E. Lutkin, G.W. McBeth, Pulse shape discrimination in inorganic and organic scintillators, I Nucl. Instrum. Methods 95 (1971) 141–153.